Reaction-Path Dynamics and Theoretical Rate Constants for the $CH_3F + Cl \rightarrow HCl + CH_2F$ Reaction by Direct Dynamics Method

Efrat Rosenman and Michael L. McKee*

Contribution from the Department of Chemistry, Auburn University, Auburn, Alabama 36849

Received April 14, 1997. Revised Manuscript Received July 11, 1997[⊗]

Abstract: Ab initio calculations were carried out for the hydrogen abstraction reaction from fluoromethane by chlorine atom. Optimized geometries and frequencies were computed at the MP2/6-31+G(d) level of theory for reactants, products, and transition state, as well as 15 points along the minimum energy path (MEP). Energies were obtained by a single-point calculation at the QCISD(T)/6-311G(d,p) and MP2/6-311+G(3df,2p) levels of theory to produce the potential energy information at the G2(MP2) level of theory. The vibrational adiabatic potential curve was found to have two barriers due to large variational effects in this system. The rate constants were calculated for the temperature range 200−700 K by using variational transition state theory (VTST) with simple tunneling corrections. While a general agreement was found with experimental values when using improved canonical VTST for most of the temperature range, the calculated Arrhenius slope was too steep in comparison to experiment for lower temperatures.

Introduction

The title reaction presents several important features that invite theoretical study. The reaction path is difficult to calculate because of the flat potential energy surface (PES), and the kinetic behavior is of special interest because of the curved temperature dependence of the rate coefficients, which was recently found experimentally. Wine and co-workers[1] measured rate constants and temperature dependence over wide temperature ranges for the $CH_3X + Cl \rightarrow HCl + CH_2X$ (X = F, Cl, Br, and I) set of reactions. One of their most prominent findings was the clear deviation from linearity in the Arrhenius plots for the whole series, except the methyl iodide case (X = I) that was studied over a smaller temperature range. In addition, there are some other experimental studies available in the literature concerning rate constants for reactions $CH_3F + Cl$,[2−6] $CH_3Cl + Cl$,[7−10] and $CH_3Br + Cl$[11] which are in good agreement with the results of Wine.

In contrast to the extensive experimental kinetic data, theoretical study had been limited to saddle-point geometries and rate constant evaluation with use of the non-variational transition state theory. Rayez *et al.*[12] characterized the transition states for the abstraction of a hydrogen atom from several fluorine- and chlorine-substituted methanes. Using the geometry and vibrational frequencies of the transition state, they calculated the corresponding activation entropy and rate constant at room temperature, which was corrected for tunneling effect by a 1D-tunneling model. Their theoretical value for the $CH_3F + Cl$ reaction was found to be three times smaller than the experimental value, measured under the same conditions.

It is well-known that the accuracy of a dynamical description of chemical reactions depends not only on the precise description of the transition state but also on the quality of the whole PES. This is particularly true for reactions with low, broad potential energy barriers, for which rate constants may be controlled by different parts of the PES at different temperatures. Such reactions require potential energy information within a wide vicinity of the energy barrier. There is no analytical PES available for the $CH_3F + Cl$ reaction; however, a very useful and convenient means to obtain kinetic data is by using *direct dynamics*.[13] Direct dynamic methods use electronic structure information, including geometries, energies, gradients, and force constants (Hessians) at selected points on the reaction path, to calculate rate constants without the intermediate stage of constructing a full analytical PES. The present study was carried out with this method in two stages: In the first stage, ab initio calculations were carried out for stationary points and for some extra points along the minimum energy path (MEP), which is the steepest descent from the saddle point toward reactants and products. In the second stage the potential energy information was input into Polyrate-Version 7.0[14] to obtain Variational Transition State Theory (VTST) rate constants and temperature dependence.

[⊗] Abstract published in *Advance ACS Abstracts,* September 1, 1997.

(1) Wine, P. H. and co-workers. To be submitted for publications.

(2) Manning, R. G.; Kurylo, M. J. *J. Phys. Chem.* **1977**, *18*, 291.

(3) Tschuikow-Rouz, E.; Yano, T.; Niedzielski, J. *J. Chem. Phys.* **1985**, *82*, 65.

(4) Tuazon, E. C.; Atkinson, R.; Corchnoy, S. B. *Int. J. Chem. Kinet.* **1992**, *24*, 639.

(5) Wallington, T. J.; Ball, J. C.; Nielsen, O. J.; Bartkiewicz, E. *J. Phys. Chem.* **1992**, *96*, 1241.

(6) De More, W. B.; Sander, S. P.; Golden, D. M.; Hampton, R. F.; Kurylo, M. J.; Howard, C. J.; Ravishankara, A. R.; Kolb, C. E.; Molina, M. J. JPL Publication 92−20; Jet Propulsion Laboratory: Pasadena, CA, 1992.

(7) Pritchard, H. O.; Pyke, J. B.; Trotman-Dickenson, A. F. *J. Am. Chem. Soc.* **1955**, *77*, 2629.

(8) Knox, J. H. *Trans. Faraday. Soc.* **1962**, *58*, 275.

(9) Clyne, M. A. A.; Walker, R. F. *J. Chem. Soc., Faraday Trans. 1* **1973**, *69*, 1547.

(10) Atkinson, R.; Baulch, D. L.; Cox, R. A.; Hampson, R. F.; Keer, J. A.; Troe, J. *J. Phys. Chem. Ref. Data* **1992**, *21* (6), 1125.

(11) Gierczak, T.; Goldfarb, L.; Sueper, D.; Ravishankara, A. R. *Int. J. Chem. Kinet.* **1994**, *26*, 719.

(12) Rayez, M.; Rayez, J.; Sawerysyn, J. *J. Phys. Chem.* **1994**, *98*, 11342.

(13) (a) Truhlar, D. G. Direct Dynamics Method for the Calculation of Reaction Rates. In *The Reaction Path in Chemistry: Current Approaches and Perspectives*; Heidrich, D., Ed.; Kluwer: Dordrecht, 1995; pp 229−255. (b) Truhlar, D. G.; Garrett, B. C.; Klippenstein, S. J. *J. Phys. Chem.* **1996**, *100*, 12771. (c) Hu, W.-P.; Truhlar, D. G. *J. Am. Chem. Soc.* **1996**, *118*, 860.

(14) Steckler, R.; Chuang, Y.-Y.; Coitino, E. L.; Hu, W.-P.; Liu, Y.-P.; Lynch, G. C.; Nguyen, K. A.; Jackels, C. F.; Zhen Gu, M.; Rossi, I.; Fast, P.; Clayton, S.; Melissas, V. S.; Garrett, B. C.; Isaacson, A. D.; Truhlar, D. G. *POLYRATE*, Version 7.0 (University of Minnesota, Minneapolis, 1996).

S0002-7863(97)01185-2 CCC: $14.00

Methods and Calculation Details

Geometries, energies, and first and second energy derivatives were calculated with the Gaussian 94 system of programs. As a reasonable compromise between speed and accuracy, the stationary point geometries (reactants, products, and saddle point) and the geometries of points along the MEP were optimized at the MP2/6-31+G(d) level of theory. Starting from the MP2 saddle-point geometries, and going downhill to both the asymptotic reactant and product channels in mass-weighted internal coordinates (with no reorientation and no use of symmetry), we constructed the intrinsic reaction path (IRC).[15] The IRC calculation was done with an even gradient step size of 0.15 bohr·amu$^{1/2}$, calculating 5 points in the product direction (up to $s = +0.75$ bohr·amu$^{1/2}$) and 10 points in the more difficult reactant channel (down to $s = -1.5$ bohr·amu$^{1/2}$). Along this energy path, the reaction coordinate s is defined as the signed distance from the saddle point, with $s > 0$ referring to the product side. In this work the units of s are bohr·amu$^{1/2}$. At each point along the MEP we computed the matrix of force constants at the MP2/6-31+G(d) level of theory, projected out the overall rotations, translations, and reaction path, and performed a generalized normal mode analysis to obtain $3N - 7$ harmonic vibrational frequencies.

After the optimization, single-point calculations of energies were carried out at the QCISD(T)/6-311G(d,p) and MP2/6-311+G(3df,2p) levels of theory. These single-point calculations were done for the stationary points as well as for the IRC to establish the electronic potential curve at the G2(MP2) level of theory. For comparison, we additionally performed single-point energy calculations for the stationary points at the G2 level of theory. We note that the G2(MP2) and G2 calculations were made with MP2/6-31+G(d) geometries and frequencies rather than the prescribed MP2/6-31G geometries and HF/6-31G(d) frequencies. The largest deviation from the correct $\langle S^2 \rangle$ value along the IRC was 0.78 (at the UMP2/6-31+G(d) level), indicating that spin contamination was not significant.

This initial information (optimized geometries, energies, gradients and frequencies along the MEP) was used to construct our ab initio PES, and allowed us to calculate the variational rate constants and to include tunneling corrections using the general polyatomic rate constant code Polyrate-7.0. We used the Improved Canonical Variational Theory (ICVT), with zero-curvature tunneling (ZCT), which is based on the minimum energy path semiclassical adiabatic ground-state (MEPSAG) method.[16] The rotational partition functions were calculated classically while the vibrational partition functions were calculated quantum mechanically within the harmonic approximation. The correlation of frequencies along the MEP was done via a diabatic scheme,[17] in which the correlation between normal modes of two different points was done manually, in accordance with the changing symmetric character of those vectors. When the vectors describing two vibrational modes of the same symmetry became mixed, we used continuity to help assign the identity of each. The importance of correlating the frequency modes diabatically, especially for rate constant calculations at low temperatures, has been pointed out by Villa *et al.*[17]

The extra information (potential energy and generalized vibrational frequencies) at intervals of 0.05 a_0, in mass-scaled Cartesian coordinates, was interpolated in Polyrate by a 3-point order Lagrange method. To establish the behavior of the MEP quantities in the asymptotic regions we used the extrapolation option[18] implemented in the code with the functional form $F(s) = A(s - B)e^{-Cs}$.

(15) Gonzalez, C.; Schlegel, H. B. *J. Phys. Chem.* **1990**, *94*, 5523 and references therein.

(16) Truhlar, D. G.; Isaacson, A. D.; Garrett, B. C. Generalized Transition State Theory. In *The Theory of Chemical Reaction Dynamics*; Baer, M., Ed.; CRC Press: Boca Raton, FL, 1985; Vol. 4, p 65.

(17) Villa, J.; Gonzalez-Lafont, A.; Lluch, J. M.; Bertran, J. *Mol. Phys.* **1996**, *89*, 633.

(18) Isaacson, A. D.; Truhlar, D. G.; Rai, S. N.; Steckler, R.; Hancock, G. C.; Garrett, B. C.; Redmon, M. J. *Comput. Phys. Comm.* **1987**, *47*, 91.

(19) *Structure of Free Polyatomic Molecules*; Landolt-Börnstein; New Series Vol. 21; Kuchitsu, K., Ed.; Springer-Verlag: New York, 1992.

(20) Huber, K. P.; Herzberg, G. *Molecular Spectra and Molecular Structure. IV Constants of Diatomic Molecules*; Van Nostrand Reinhold Co.: New York, 1979.

Table 1. MP2/6-31+G(d) Optimized Geometries[a] for the Reactant, Products, and Saddle Point for the $CH_3F + Cl$ Reaction

parameter	CH_3F	CH_3FCl (TS)	CH_2F	HCl
r(CH)	1.090 (1.086)[b]	1.088 [1.078][c]	1.081 (1.090)[b]	
r(CH′)		1.403 [1.349]		
r(CF)	1.407 (1.383)	1.356 [1.326]	1.361 (1.334)	
r(H′Cl)		1.450 [1.500]		1.281 (1.275)[d]
∠HCH	110.9 (110.2)	119.2	123.4 (126.3)	
∠FCH	108.0 (108.8)	112.1 [107.6]	113.4	
∠FCH′		105.9 [102.7]		
∠CH′Cl		179.8		
$L = \delta r_{CH'}/\delta r_{H'Cl}$		1.852 [1.134]		

[a] Bond lengths are expressed in angstroms, angles in degrees. [b] Values in parentheses are experimental values from ref 19. [c] Values in brackets are theoretical results from ref 12, obtaining at the HF/6-31G(d,p) level of theory. [d] Value in parentheses is an experimental value from ref 20.

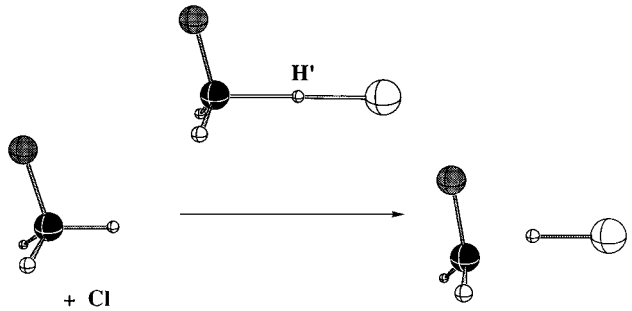

Figure 1. MP2/6-31+G(d) optimized geometries of CH_3F, CH_2F, and the saddle point.

Results and Discussion

A. The Stationary Points. The optimized geometric parameters of the reactant, products, and transition state (meaning the conventional transition state at $s = 0$) are given in Table 1, and the corresponding structures are given in Figure 1 for the hydrogen abstraction reaction at the MP2/6-31+G(d) level of theory. Table 1 also reports the available experimental values for CH_3F, CH_2F, and HCl (in parentheses). The theoretical C−F bond length differs from the experimental values by up to 0.027 Å (r(C−F) for CH_2F), while the largest deviation for the C−H bond lengths is 0.009 Å (r(C−H) for CH_2F). The calculated FCH angle differs from the experimental value by 0.8° (CH_3F), and the calculated HCH angles differ from the experimental values by up to 2.9° (CH_2F). These results are in good agreement with another study of Glukhovtsev *et al.*,[21] where they noted that MP2 calculations with larger basis sets (e.g. 6-311+G(2df,p)) gave quite precise agreement with experimental geometries for CH_3X (X = F, Cl, Br, and I) systems.[22] Rayez *et al.*[12] calculated reactions RH + Cl → R + HCl (R is a halogen-substituted hydrocarbon) at the HF/6-31G** level of theory. Their results for the transition state of $H_2FC-H-Cl$ are included in Table 1 (brackets). The bond length between the carbon and the abstracted hydrogen (r(C−H′)) is calculated by the current study to be shorter by 0.054 Å than the same bond length reported by Rayez *et al.*, while the calculated bond length of r(H′−Cl) is larger by 0.05 Å. These differences are incorporated into the parameter L, which is shown in the last row of Table 1. This parameter is the ratio between the elongation of the C−H′ bond and the elongation of the H′−Cl bond: $L = \delta r$(C−H′)/δr(H′−Cl) and represents the reactant- or product-like character of the forming transition state. It can be seen that both calculations provide $L > 1$; that is to say, the

(21) Glukhovtsev, M. N.; Pross, A.; Radom, L. *J. Am. Chem. Soc.* **1995**, *117*, 2024.

(22) Gauld, J. W.; Radom, L. *J. Phys. Chem.* **1994**, *98*, 777.

Table 2. Enthalpies of Activation, $\Delta H_r^{\#}$, and Enthalpies of Reaction, ΔH_r, Calculated at the G2(MP2) and G2 Levels of Theory for the $CH_3F + Cl$ Reaction

	ΔH_r (kcal/mol)		$\Delta H_r^{\#}$ (kcal/mol)		
level	0 K	298 K	0 K	298 K	E_a (kcal/mol)[a]
MP2	+6.6		12.5		
G2(MP2)	−2.2	−2.9	1.6	0.6	1.2
G2	−1.3	−1.0	2.3	1.4	2.0
BAC-MP4		−2.6[b]		2.2[b]	3.4[b]
exp		−3.1[c]			1.5 ± 1[d]

[a] Activation energy at 298 K. [b] Ab initio study for 300 K from ref 12. [c] Experimental value for 298 K from ref 10. [d] Experimental value from ref 6.

transition state is reactant-like, but this reactant-like character is more pronounced in the present study ($L = 1.85$ with G2(MP2) compared to 1.13 with HF/6-31G**). The geometry predicted for the transition state is collinear with regard to the angle between the breaking C−H′ bond and the nascent H′−Cl bond ($\angle$CH′Cl = 179.8°), as was observed for a similar reaction of $CH_4 + Cl$.[23] It can also be noticed that the C−F "spectator bond", which is not involved in the reaction, is shortened at the transition state while the C−H′ breaking bond is elongated.

Calculated enthalpies at 0 and 298 K (including heat capacity corrections obtained from MP2/6-31+G(d) unscaled frequencies) for the stationary points at the G2(MP2) and G2 levels of theory are available as Supporting Information in Table S1. On the basis of Table S1, enthalpies of reaction and enthalpies of activation were calculated at the MP2, G2(MP2), and G2 levels of theory, and are shown in Table 2 along with BAC-MP4 results from ref 12 and experimental values for comparison. We should note that the G2(MP2) and G2 energies are obtained with a nonstandard method. Specifically, we calculated the geometries at the MP2/6-31+G(d) level (rather than MP2/6-31G(d)) and calculated zero-point energies at the MP2/6-31+G(d) level with a 0.93 weighting factor (rather than HF/6-31G(d) with a 0.8929 factor). One of the most prominent findings in Table 2 is the overestimation of the barrier at the MP2 level of theory. At 0 K, the MP2 enthalpy barrier is 12.5 kcal/mol, which can be compared to the G2(MP2) enthalpy barrier (at 0 K) of 1.6 kcal/mol or the G2 enthalpy barrier (at 0 K) of 2.3 kcal/mol. The experimental activation energy is 1.5 ± 1.0 kcal/mol[6] (see Table 2). It is also shown that the MP2 calculation predicts the reactions to be endothermic, while the higher two levels find the reaction to be exothermic. The best agreement between theory and experiment, from the exoergicity point of view, is obtained by the G2(MP2) level of theory.

B. The Reaction Paths. Intrinsic reaction coordinate calculations in the vicinity of the transition state provide geometries, which were used to compute gradients and frequencies at the MP2 level of theory and single-point energies at the higher G2(MP2) level of theory. Figure 2 presents the ground-state vibrationally adiabatic potential energy surface,

$$V_a^G(s) = V_{MEP}(s) + E_{int}(s)$$

where V_{MEP} is the classical potential energy path (the G2(MP2) electronic profile) and E_{int} is the local zero-point energy (ZPE), as a function of s, for the reaction under study. In addition, the basic MP2 electronic curve is also shown. This figure is essential for understanding the dynamic behavior of this system so we will discuss its important features.

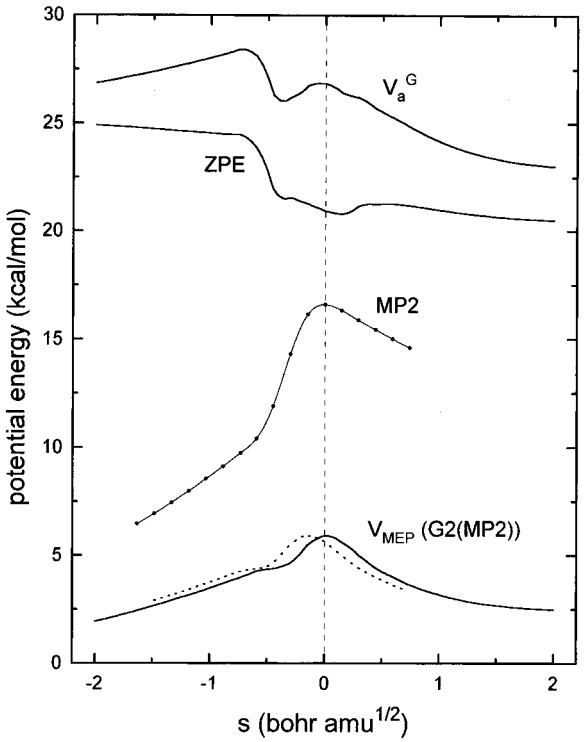

Figure 2. Classical potential energy curve (V_{MEP}) calculated at the G2(MP2) level, zero-point energies (ZPE), and vibrationally adiabatic potential energy curve (V_a^G) as a function of the reaction coordinate, s. The MP2 electronic energies are also plotted and can be compared with the G2(MP2) electronic energies (V_{MEP}).

We would like to emphasize three points. First, as was demonstrated in Table 2, the electronic curve at the MP2 level of theory describes an endothermic reaction with a steep barrier, while this reaction is actually expected to have a low barrier with a flat entrance valley. Second, the G2(MP2) electronic curve, V_{MEP}, is reasonably flat, and the maximum is shifted toward the reactants to approximately $s = -0.15$ bohr·amu$^{1/2}$ (see dotted V_{MEP} line). Espinosa-Garcia and Corchado[24] have argued that this kind of shifting is artificially caused by the computational technique, which consists of optimizing geometries at a lower level A (here A is MP2) and then calculating the energies (without re-optimization) at a higher level B (here B is G2(MP2)). They suggested moving the maximum of the single-point calculation curve, B//A, to its original position ($s = 0$ for the A//A level), thus avoiding a conceptual mistake of taking as a variational effect what is only a numerical defect. It should be noticed that according to this procedure the frequencies are not shifted, i.e. each geometry at the A//A level should correspond to its original frequencies (calculated at the A//A level) and to a shifted energy (calculated at the B//A level). We applied this modification and used shifted curves as our electronic PES (solid V_{MEP} lines).

Finally and most importantly, due to a significant drop in the zero-point energy (ZPE) curve prior to the saddle point zone, the overall ground-state vibrationally adiabatic PES, $V_a^G(s)$, possesses two barriers: one, higher in energy, in the entrance valley at approximately $s = -0.73$ bohr·amu$^{1/2}$, and another one at the original transition state at $s = 0$. A two-barriers shape of V_a^G, which was also found for the $CH_3 + D_2$ and $CH_3 + HD$ isotopic reactions,[25] is a consequence of summing up V_{MEP} and ZPE curves. The shape of V_{MEP} is well established, and the ZPE curve is composed of contributions from all the vibrational modes.

(23) Truong, T. N.; Truhlar, D. G.; Baldridge, K. K.; Gordon, M. S.; Steckler, R. *J. Chem. Phys.* **1989**, *90*, 7137.
(24) Espinosa-Garcia, J.; Corchado, J. C. *J. Phys. Chem.* **1995**, *99*, 8613.
(25) Corchado, J. C.; Espinosa-Garcia, J. *J. Chem. Phys.* **1997**, *106*, 4013.

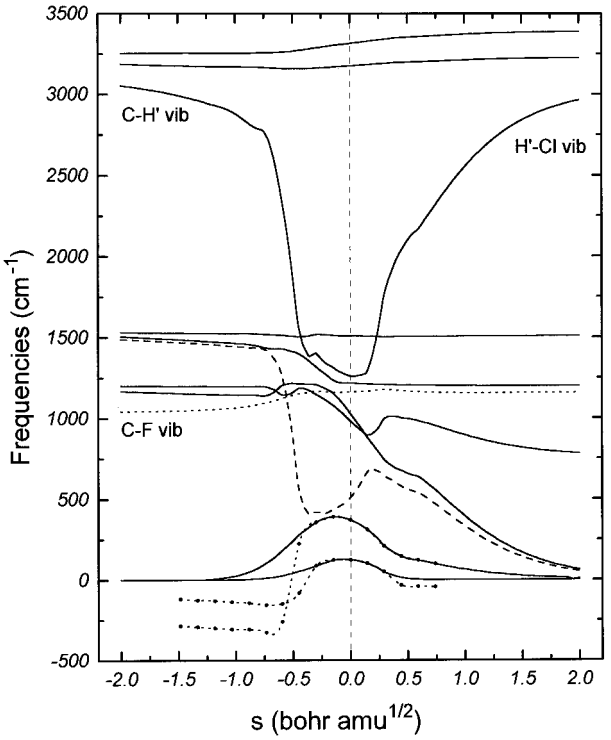

Figure 3. Generalized normal-mode vibrational frequencies as a function of the reaction coordinate, *s*. Imaginary values are represented by negative values.

To analyze the behavior of the ZPE curves, Figure 3 shows the variation of the generalized normal mode frequencies along the reaction path. In the negative limit of *s* ($s = -\infty$), there are nine frequencies corresponding to the CH_3F reactant. As one approaches the saddle point zone, two vibrational modes drop sharply: the harmonic vibrational frequency of the C−H′ stretch (solid line), corresponding to the normal mode breaking during the reaction and correlating with the H′−Cl stretching at the product, and the symmetric bending frequency of the H−C−H′ (dashed line), which goes to zero after the transition state (the reacting H′ departs from CH_3F). This frequency (the symmetric bending) has a minimum for *s* around −0.3 bohr·amu$^{1/2}$, which did not seem to exist for the $NH_3 + H$ reaction[25,26] where the calculations had been done in curvilinear coordinates. To check whether this minimum is due to the use of rectilinear coordinates, we carried out the normal mode analysis in curvilinear coordinates and found the same minimum for this vibrational mode (a table with the rectilinear frequencies as well as the curvilinear values for the symmetric bending mode (ν_9) is available as Supporting Information (Table S2)).

On the other hand, the two lowest harmonic frequencies, corresponding to free rotations and translations that evolve into vibrations (transitional modes), present a maximum coinciding with the minimum of the reactive modes and fall to zero toward reactants and products. However, the behavior of these transitional modes does not fully compensate the fall of the reactive modes, and thus the ZPE shows a noticeable drop with *s*. This kind of drop in the ZPE profile is not unique and it characterizes hydrogen abstraction reactions (see, for example, $NH_3 + H \leftrightarrow NH_2 + H_2$, refs 26 and 27), but when combined with a low, broad classical barrier profile, it causes a large shift of the variational transition state, i.e. a large variational effect.

At this point we would like to further discuss the translational modes, which became imaginary outside the range of *s*: (−0.4) to (0.4) bohr·amu$^{1/2}$ (see dotted lines of the two lowest modes in Figure 3). Before doing any modifications, we wanted to make sure that the variations of the frequencies along the path were correct, and do not indicate that our potential curve is off the MEP. We recalculated the path for the $CH_3F + Cl$ reaction, using a 15 times smaller step size (our original coarse grid used a step size of 0.15 bohr·amu$^{1/2}$, while the fine check grid used a step size of 0.01 bohr·amu$^{1/2}$). Table 3 compares calculated frequencies of the coarse and fine grids, at six points around the saddle point (three in each direction). It is clearly shown that the differences between the two grids are minor, and that imaginary, unphysical frequencies are produced outside the range of $-0.4 < s < 0.4$, even when using a much smaller step size to compute the MEP (thus our set of points is, at least, a good approximation to the reaction path). It is known that for points along the MEP different from the stationary points, where the gradient is nonzero, the harmonic vibrational frequencies are dependent on the choice of coordinates.[28−30] Several studies[31−32] have demonstrated that the more physical curvilinear coordinate system can remove this common problem of unphysical imaginary frequencies. However, the approach we used in the present study to correct the imaginary values was the one suggested by Gonzalez-Lafont *et al.*,[33] according to which we fit the frequencies to a simple analytical expression, based on their values at the stationary points and two other points at each side of the saddle point. The corrected vibrational modes are shown as solid lines in Figure 3.

Table 3. Comparison of Relative Energies (kcal/mol), Transitional Frequencies (cm^{-1}), and Zero-Point Energies (kcal/mol) between Fine and Coarse Grids for the $CH_3F + Cl \rightarrow HCl + CH_2F$ Reaction

	relative energy[a]		V_1		V_2		ZPE	
s	fine	coarse	fine	coarse	fine	coarse	fine	coarse
−0.45	11.65	11.90	−94.8	−81.6	185.9	221.6	21.85	21.78
−0.30	14.04	14.32	77.8	86.3	348.0	356.9	21.58	21.55
−0.15	15.99	16.60	120.0	122.1	389.6	390.0	21.30	21.26
0.15	16.28	16.33	94.9	101.9	295.6	310.3	20.83	20.79
0.30[b]	15.80	15.87	36.4	48.5	194.5	209.8	21.21	21.17
0.45[c]	15.40	15.44	−32.5	−34.6	146.0	144.8	21.26	21.24

[a] MP2 total energies relative to the total energy of the reactants. [b] Value of the coarse grid is 0.29. [c] Value of the coarse grid is 0.44.

The importance of having "well-behaved" translational modes is not due to their effect on the vibrational adiabatic potential curve, $V_a^G(s)$, which is found to be very small, but due to the deceptive influence of the imaginary values on the free energy of the activation profile. In variational transition state theory,[16] the dividing surface corresponds to the maximum of $\Delta G^{GT,0}(T,s)$ for a given temperature *T*. The calculation of $\Delta G^{GT,0}(T,s)$ requires carrying out generalized normal mode analysis at nonstationary points along the path, or having the corresponding vibrational frequencies as input. Figure 4 shows the change of $\Delta G^{GT,0}(T,s)$ along IRC for the $CH_3F + Cl$ reaction calculated by Polyrate-7.0 using the corrected frequencies, in the temperature range of 200−750 K. As seen in Figure 4, the ΔG curves exhibit an oscillatory change along the reaction coordinate in the vicinity of the two barriers, discussed earlier. Such oscillations in ΔG curves were also reported for the $NH_3 +$

(26) Espinosa-Garcia, J.; Corchado, J. C. *J. Chem. Phys.* **1994**, *101*, 1333.
(27) Natanson, G. A. *Chem. Phys. Lett.* **1992**, *190*, 209.
(28) Natanson, G. A. *Chem. Phys. Lett.* **1992**, *190*, 215.
(29) Jackels, C. F.; Gu, Z.; Truhlar, D. G. *J. Chem. Phys.* **1995**, *102*, 3188.
(30) Nguyen, K. A.; Jackels, C. F.; Truhlar, D. G. *J. Chem. Phys.* **1996**, *104*, 6491.
(31) Natanson, G. A.; Garrett, B. C.; Truong, T. N.; Joseph, T.; Truhlar, D. G. *J. Chem. Phys.* **1991**, *94*, 7875.
(32) Espinosa-Garcia, J.; Corchado, J. C. *J. Phys. Chem.* **1996**, *100*, 16561.
(33) Gonzalez-Lafont, A.; Truong, T. N.; Truhlar, D. G. *J. Chem. Phys.* **1991**, *95*, 8875.

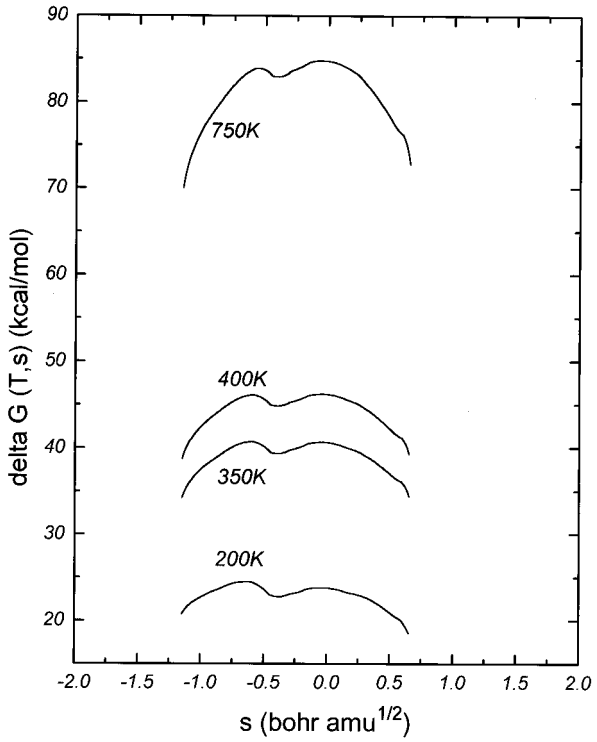

Figure 4. Changes of improved generalized free energy of activation as a function of the reaction coordinate, *s*, at different temperatures.

Table 4. Bottleneck Properties of the $CH_3F + Cl \rightarrow HCl + CH_2F$ Reaction[a]

T (K)	*s*	V_{MEP}	V_a^G
s.p.	0.0	5.90	26.85
200.0	−0.641	4.17	28.27
350.0	−0.606	4.24	28.14
373.0	−0.602	4.25	28.12
374.0	−0.045	5.82	26.86
400.0	−0.046	5.82	26.86
600.0	−0.05	5.80	26.86

[a] Based on the ICVT method.

$NO \rightarrow NH_2 + HNO$ reaction,[34] and they are attributed to the entropy factor in the Gibbs free energy.

C. Rate Constants. Table 4 lists the dynamic bottleneck (s*) properties of the $CH_3F + Cl$ reaction, based on the improved canonical approach (ICVT). It is interesting to see that in accordance with the shape of the free energy curve (Figure 4), there are two "groups" of general transition states (GTS). At low temperatures, (specifically $T \leq 373$ K), the left peak of $\Delta G^{GT,0}(T,s)$ is higher, and the GTS are strongly shifted away from the saddle point toward the reactants ($s^* \approx -0.6$ bohr·amu$^{1/2}$). At high temperatures ($T \geq 374$ K) the right peak becomes dominant, and the GTS, although still in the entrance valley, are much closer to the saddle point. The bottleneck properties indicate that for the low-temperature range the variational effects are large, and that for this low barrier reaction, entropy considerations control the location of the GTS, as was demonstrated for other low barrier reactions (for example $CH_4 + F \rightarrow HF + CH_3$[35]).

Figure 5 shows the conventional (TST), the variational (ICVT), and the experimental Arrhenius plots and rate constants for the $CH_3F + Cl$ reaction, in the temperature range of 200−700 K. Conventional TST (dashed line) overestimated the experimental value for all the temperature range, from 22% at

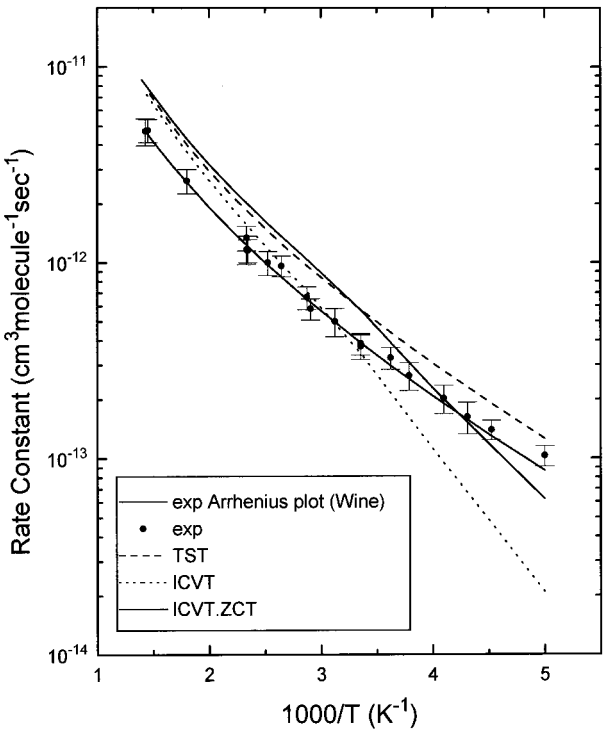

Figure 5. Computed TST, ICVT, and ICVT(ZCT) rate constants as a function of $10^3/T$ for the $CH_3F + Cl$ reaction. Experimental values and the Arrhenius plot were measured by Wine *et al.* (ref 1).

200 K (1.26×10^{-13} compared with 1.03×10^{-13} for TST and experiment, respectively) to 66% at 699 K, which is the highest experimental temperature studied (78.1×10^{-13} compared with 46.9×10^{-13} for TST and experiment, respectively). The TST slope is in general agreement with the curved experimental plot. As for ICVT results (dotted line), the Arrhenius plot is composed of two contributions, in accordance with the discussion in the previous paragraph. The lower temperature range gives rise to steeper slope due to higher barriers at the more shifted bottlenecks, while for the higher temperature range the calculated ICVT rate constants are governed by GTS, which are located very close to the conventional transition state (at $s \cong -0.05$), so the ICVT values are quite similar to the TST values, as temperatures go higher. The ICVT rate constants are within the experimental uncertainties for temperatures between 290 and 450 K; they are somewhat too large for higher temperatures, and too small for the low range. When dealing with hydrogen transfer reactions like the present one, tunneling corrections are expected to enhance the rate of reaction, especially at low temperature, which would improve the agreement between theory and experiment for this range. We included tunneling through zero curvature corrections (MEPSAG), and the results are shown in Figure 5 (solid line, ICVT(ZCT)). The numerical agreement between the ICVT(ZCT) and the experimental values is rather good (the differences are less than 50% for the whole temperature range), but the slope of the calculated ICVT(ZCT) Arrhenius plot at the low- temperature range is too steep. One possible cause for this deviation could be that the relative heights of the first and second barriers are not accurate. It is possible that a slightly higher first barrier (the one located at $s = -0.05$ bohr·amu$^{1/2}$) and a slightly lower second barrier (the shifted one at $s = -0.73$ bohr·amu$^{1/2}$) could provide a better agreement with experiment.

Conclusions

An ab initio study for the $CH_3F + Cl \rightarrow HCl + CH_2F$ abstraction reaction has been performed by using single-point

(34) Mebel, A. M.; Diau, E. W. G.; Lin, M. C.; Morokuma, K. *J. Phys. Chem.* **1996**, *100*, 7517.

(35) Corchado, J. C.; Espinosa-Garcia, J. *J. Chem. Phys.* **1996**, *105*, 3152.

calculations at the G2(MP2) level of theory. The vibrationally adiabatic potential energy surface was found to have two maxima, one close to the conventional transition state at $s = -0.05$ bohr·amu$^{1/2}$, and a second one, higher in energy, further away from the transition state into the reactant valley, at $s = -0.73$ bohr·amu$^{1/2}$. This nonregular shape was attributed to the combination of two different factors: the low energy barrier and the relatively large early drop in the zero-point energies prior to the saddle point zone, which was caused mainly by changes of two vibrational frequencies along the reaction path (the C−H′ stretching vibration corresponding to the bond which breaks during the reaction and correlates with the H′−Cl stretch of the product, and the symmetric H−C−H′ bending frequency which goes to zero after the transition state). The asymmetric character of the vibrational modes as a function of s is responsible for the early drop in the ZPE curve. The present study suggests that the characteristic two-barrier shape of the vibrationally adiabatic potential curve is likely to be found in asymmetric hydrogen abstraction reactions with low classical barriers. The drop in the ZPE curve can be significant, and when combined with a low barrier can cause marked variational effects in the reaction.

The potential energy information was used with Polyrate-Version 7.0 to produce VTST rate constants over the range 200−700 K, for which there are experimental data. The calculated TST rate constants were too large over the whole temperature range, while ICVT rates were within the experimental uncertainties at 290−450 K and too small at lower temperatures. Zero-curvature tunneling corrections to the rate coefficients caused an increase of the rate constants at low temperatures and thus improved the agreement with experiment. However, the calculated Arrhenius slope at low temperatures was found to be too steep, in comparison to the experimental behavior.

In the present reaction, the agreement between theory and experiment is not sufficient to confirm the double-barrier potential. However, work is in progress on the reactions $CH_3X + Cl$ (X = Cl, Br, and I) where we are exploring the dual-level reaction path dynamic method.[36−38] Preliminary results indicate that the two-barrier shape of the vibrational adiabatic potential is also present in all three reactions.

Acknowledgment. We thank Dr. Don Truhlar and Dr. Rozeanne Steckler for providing the Polyrate 7.0 program and for helpful conversations. We thank Dr. Paul Wine for sharing data on the $CH_3F + Cl \rightarrow HCl + CH_2F$ reaction. Computer time was provided by the Alabama Supercomputer Network. E. R. would like to thank Boaz Rosenman for his support.

Supporting Information Available: Total energies and enthalpies of various species are given in Table S1 at the G2(MP2) and G2 levels; Table S2 gives a tabulation of vibrational frequencires calculated along the IRC in curvilinear coordinates as well as a comparison with the bending mode (ν_9) calculated in rectilinear coordinates (3 pages). See any current masthead page for ordering and Internet access instructions.

Note Added in Proof: Attention is drawn to a recent development in the diabatic ordering of vibrational normal modes which will improve and simpify direct dynamics studies such as this one. See: Konkoli, Z.; Cremer, D.; Kraka, E. *J. Comput. Chem.* **1997**, *18*, 1282.

JA971185L

(36) Hu, W.-P.; Liu, Y.-P.; Truhlar, D. G. *J. Chem. Soc., Faraday. Trans.* **1994**, *90*, 1715.
(37) Corchado, J. C.; Espinosa-Garcia, J.; Hu, W.-P.; Rossi, I.; Truhlar, D. G. *J. Phys. Chem.* **1995**, *99*, 687.
(38) Chuang, Y.-Y.; Truhlar, D. G. *J. Phys. Chem. A* **1997**, *101*, 3808.